EVIDENTIAL TURING PROCESSES

Anonymous authors
Paper under double-blind review

ABSTRACT

A probabilistic classifier with reliable predictive uncertainties i) fits successfully to the target domain data, ii) provides calibrated class probabilities in difficult regions of the target domain (e.g. class overlap), and iii) accurately identifies queries coming out of the target domain and reject them. We introduce an original combination of Evidential Deep Learning, Neural Processes, and Neural Turing Machines capable of providing all three essential properties mentioned above for total uncertainty quantification. We observe our method on four classification tasks to be the only one that can excel all three aspects of total calibration with a single standalone predictor. Our unified solution delivers an implementation-friendly and compute+efficient recipe for safety clearance and provides intellectual economy to an investigation of algorithmic roots of epistemic awareness in deep neural nets.

1 INTRODUCTION

The applicability of deep neural nets to safety-critical use cases such as autonomous driving or medical diagnostics is still a matter of fundamental research (Schwalbe & Schels, 2020). Key challenges in the development of total safety in deep learning are at least three-fold: i) evaluation of model fit, ii) risk assessment in difficult regions of the target domain (e.g. class overlap) based on which safety-preserving fallback functions can be deployed, and ii) rejection of inputs that do not belong to the target domain, such as an image of a cat presented to a character recognition system.

The attention of the machine learning community on each of these critical safety elements is in steady increase (Naeini et al., 2015; Guo et al., 2017; Kuleshov et al., 2018). However, the developments follow isolated directions and the proposed solutions are largely fragmented. Calibration of neural net probabilities focuses primarily on post-hoc adjustment algorithms trained on validation sets from in-domain data (Guo et al., 2017), ignoring the out-of-domain detection and model fit evaluation aspects. On the other hand, recent advances in out-of-domain detection build on strong penalization of divergence from the probability mass observed in the target domain (Sensoy et al., 2018; Malinin & Gales, 2018), distorting the quality of class probability scores. Such fragmentation of best practices not only hinders their accessibility by real-world applications but also complicates the scientific inquiry of the underlying reasons of sub-optimality of neural net uncertainties.

We aim to identify the guiding principles for Bayesian modeling that deliver the most complete set of uncertainty quantification capabilities in one single model. We first characterize Bayesian models with respect to the relationship of their global and local variables: (a) *Parametric Bayesian Models* comprise a likelihood function that maps inputs to outputs via probabilistic global parameters, (b) *Evidential Bayesian Models* apply an uninformative prior distribution on the parameters of the likelihood function and infer the prior hyperparameters by amortizing on an input observation. Investigating the decomposition of predictive distribution variance, we find out that the uncertainty characteristics of these two approaches exhibit complementary strengths. We introduce a third approach that employs a prior on the likelihood parameters that both conditions on the input observations on the true model and amortizes on them during inference. The mapping from the input observations to the prior hyperparameters is governed by a random set of global parameters. We refer to the resulting approach as (c) *Complete Bayesian Models*, as we find out that its predictive distribution variance combines the favorable properties of Parametric and Evidential Bayesian Models. Figure 1 gives an overview of the relationship between these three Bayesian modeling approaches.

The advantage of the Complete Bayesian Models come with the challenge of choosing an input-dependent prior. We introduce a new stochastic process construction that addresses this problem

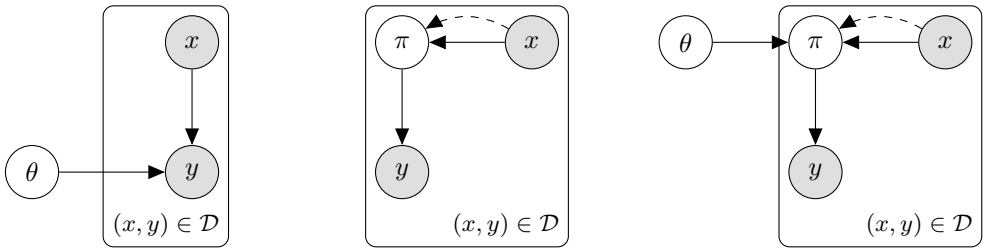

(a) Parametric Bayesian Model (b) Evidential Bayesian Model (c) Complete Bayesian Model

Figure 1: Plate diagrams of three main Bayesian modeling approaches. Shaded nodes are observed and unshaded ones are latent. The solid direct arrows denote conditional dependencies in the true model, while the bent dashed arrows denote amortization in variational inference.

by accumulating observations on a context set during training time into the parameters of a global hyperprior variable by an explicitly designed update rule. We design the input-specific prior on the likelihood parameters by conditioning it on both the hyperprior and the input observation. As conditioning via explicit parameter updates amounts to maintaining an external memory that can be queried by the prior distribution, we refer to the eventual stochastic process as a *Turing Process* with inspiration from the earlier work on Neural Turing Machines (Graves et al., 2014) and Neural Processes (Garnelo et al., 2018b). We arrive at our target Bayesian design that is equipped with the complete set of uncertainty quantification capabilities by incorporating the Turing Process design into a Complete Bayesian Model. We refer to the resulting approach as an *Evidential Turing Process*. We observe on four real-world classification tasks that the Evidential Turing Process is the only model that excels simultaneously at model fit, class overlap quantification, and out-of-domain detection.

2 Problem Statement: Total Calibration

Consider the following data generating process with K modes

$$y|\pi \sim Cat(y|\pi), \qquad x|y \sim \sum_{k=1}^{K} \mathbb{I}_{y=k} p(x|y=k) \tag{1}$$

where $Cat(y|\cdot)$ is a categorical distribution and $p(x|y)$ is the class-conditional density function. For any fixed prior class distribution π, the classification problem can be cast as identifying the class probabilities for observed patterns $Pr[y|x, \pi] = \mathrm{Cat}(y|f^{\pi}_{true}(x))$ where $f^{\pi}_{true}(x)$ is a $K-$dimensional vector with $k-$th element

$$f^{\pi,k}_{true}(x) = \pi_k p(x|y=k) \Big/ \sum_{k=1}^{K} \pi_k p(x|y=k). \tag{2}$$

In most real-world cases f^{π}_{true} is not known and should be identified from a hypothesis space $h_\pi \in \mathcal{H}_\pi$ via inference from a set of samples $\mathcal{D} = \{(x_n, y_n)|n = 1, \ldots, N\}$ obtained from the true distribution. The risk of the Bayes classifier $\mathrm{argmax}_y Cat(y|h_\pi(x))$ for a given input x is

$$R(h_\pi(x)) = \sum_{k=1}^{K} \mathbb{I}_{h_\pi(x)=k} \sum_{\kappa=1}^{K} \mathbb{I}_{\kappa \neq h_\pi(x)} f^{\pi,\kappa}_{true}(x). \tag{3}$$

For the whole data distribution, we have $R(h_\pi) = \mathbb{E}_{x|\pi}[R(h_\pi(x))]$. The optimal case is when $h_\pi(x) = f^{\pi}_{true}(x)$, which brings about the irreducible Bayes risk resulting from class overlap:

$$R_*(f^{\pi}_{true}(x)) = \min\Big\{1 - \max f^{\pi}_{true}(x), \max f^{\pi}_{true}(x)\Big\}. \tag{4}$$

Total Calibration. Given a set of test samples $\mathcal{D}_{ts}$ coming from the true data generating process in Eq. 1, we define *Total Calibration* as the capability of a discriminative predictor $h_\pi(x)$ to quantify the below three types of uncertainty quantification simultaneously:

i) Model misfit evaluated by the similarity of $h_\pi(x)$ and $f^\pi_{true}(x)$ measurable directly via

$$KL(Cat(y|f^\pi_{true}(x))p(x))||Cat(y|h_\pi(x))p(x))) = \mathbb{E}_{p(x)}[\log Cat(y|f^\pi_{true}(x)] + \mathbb{E}_{p(x)}[-\log Cat(y|h_\pi(x))]$$

where $KL(\cdot||\cdot)$ denotes the Kullback-Leibler divergence. Since $\mathbb{E}_{p(x)}[\log Cat(y|f^\pi_{true}(x))]$ is a constant with respect to $h_\pi(x)$, an unbiased estimator of the relative goodness of an inferred model is the negative test log-likelihood $NLL(h_\pi(x)) = -1/|\mathcal{D}_{ts}| \sum_{(x,y)\in\mathcal{D}_{ts}} \log Cat(y|h_\pi(x))$.

ii) Class overlap evaluated by $R_*(f^\pi_{true}(x))$. As there is no way to measure this quantity from $\mathcal{D}_{ts}$, it is approximated indirectly via *Expected Calibration Error (ECE)*

$$ECE[h_\pi] = \sum_{m=1}^{M} \frac{|B_m|}{N} \Big| acc(B_m) - conf(B_m) \Big|$$

where $B_m = \{(n|h_\pi(x_n) \in [(m-1)/M, m/M]\}$ are M bins that partition the test set $\mathcal{D}_{ts} = B_1 \cup \ldots \cup B_M$ and are characterized by their accuracy and confidence scores

$$acc(B_m) = \frac{1}{|B_m|} \sum_{n\in B_m} \mathbb{I}_{y_n = \text{argmax } h_\pi(x_n)}, \qquad conf(B_m) = \frac{1}{|B_m|} \sum_{n\in B_m} h_\pi(x_n). \tag{5}$$

iii) Domain mismatch defines the rarity of an input pattern x_* for the target task, i.e. $Pr[p(x := x_*) < \epsilon]$ for small ϵ. This quantity cannot be measured since $p(x)$ is unknown. It is approximated indirectly by the success of discriminating between samples x_* coming from a different data distribution and those in $\mathcal{D}_{ts}$ by calculating the Area Under ROC (AUROC) curve with respect to $h_\pi(x_n)$.

3 Uncertainty Quantification with Parametric and Evidential Bayesian Models

Parametric Bayesian Models. A commonplace design choice is to build the hypothesis space for equipping the hypothesis function with a global parameter θ that takes values from a feasible set Θ, that is $\mathcal{H}_\pi = \{h^\theta_\pi(x)|\theta \in \Theta\}$. *Parametric Bayesian Models (PBMs)* employ a prior belief $\theta \sim p(\theta)$, which is updated after Bayesian inference on a training set $\mathcal{D}_{tr}$ as $p(\theta|\mathcal{D}_{tr}) = \prod_{(x,y)\in\mathcal{D}_{tr}} Cat(y|h^\theta_\pi(x))p(\theta)/p(\mathcal{D}_{tr})$. Consider the update on the posterior belief

$$p(\theta|\mathcal{D}_{tr} \cup (x_*, y_*)) = Cat(y_*|h^\theta_\pi(x_*))p(\theta|\mathcal{D}_{tr})/Z, \tag{6}$$

after a new observation (x_*, y_*) where the normalizer can be expressed as

$$Z = \frac{1}{p(\mathcal{D}_{tr})} \int Cat(y_*|h^\theta_\pi(x_*))L(\theta)p(\theta)d\theta. \tag{7}$$

with $L(\theta) = \prod_{(x,y)\in\mathcal{D}_{tr}} Cat(y|h^\theta_\pi(x))$. This can be seen as an inner product between functions $Cat(y_*|h^\theta_\pi(x_*))$ and $L(\theta)$ on an embedding space modulated by $p(\theta)$. As sample size grows, it will become more likely that the regions with $\max_\theta Cat(y_*|h^\theta_\pi(x_*))$ and $L(\theta)$ will superpose causing Z to increase, which will in turn make $p(\theta|\mathcal{D}_{tr} \cup (x_*, y_*))$ increasingly more peaked, that is

$$\lim_{|\mathcal{D}_{tr}|\to+\infty} Var[\theta|\mathcal{D}_{tr}] = 0. \tag{8}$$

This conjecture depends on the assumption that a single random variable θ modulates all samples. The variance of a prediction in favor of a class k decomposes according to the law of total variance

$$Var[y_* = k|x_*, \mathcal{D}] = \underbrace{Var_{\theta\sim p(\theta|\mathcal{D}_{tr})}[h^\theta_{\pi,k}(x_*)]}_{\text{Reducible model uncertainty}} + \underbrace{\mathbb{E}_{\theta\sim p(\theta|\mathcal{D}_{tr})}\Big[(1 - h^\theta_{\pi,k}(x_*))h^\theta_{\pi,k}(x_*)\Big]}_{\text{Data uncertainty}}. \tag{9}$$

Due to the Eq. 8, the first term on the r.h.s. vanishes to zero in the large sample regime and the second one coincides with the asymptotic solution of the maximum likelihood estimator θ_{MLE}. In cases when $\mathcal{H}_\pi$ contains $f^\pi_{true}(x)$, an exact inference scheme recovers it and we get

$$\lim_{N\to+\infty} \mathbb{E}_{\theta\sim p(\theta|\mathcal{D}_{tr})}\Big[(1 - h^\theta_{\pi,k}(x))h^\theta_{\pi,k}(x_*)\Big] = (1 - h^{\theta_{MLE}}_{\pi,k}(x_*))h^{\theta_{MLE}}_{\pi,k}(x_*) = (1 - f^\pi_{true}(x_*))f^\pi_{true}(x_*).$$

The simple fact below sheds light on the meaning of this result.

Proposition. *The following inequality holds for any* $\pi, \pi' \in [0.5, 1]$ *pair*

$$\min(1-\pi, \pi) \geq \min(1-\pi', \pi') \Rightarrow (1-\pi)\pi \geq (1-\pi')\pi'.$$

Proof. Define $\pi = 0.5+\epsilon$ and $\pi' = 0.5+\epsilon'$ for $\epsilon, \epsilon' > 0$. As $\min(1-\pi, \pi) \geq \min(1-\pi', \pi') \Rightarrow \epsilon \leq \epsilon'$, we get $(1-\pi)\pi = (1-0.5-\epsilon)(0.5+\epsilon) = 0.25-0.25\epsilon-\epsilon^2 \geq 0.25-0.25\epsilon'-\epsilon'^2 = (1-\pi')\pi' \square$

The conclusion is that $(1-f^{\pi}_{true}(x))f^{\pi}_{true}(x) \propto R_*(f^{\pi}_{true}(x))$. Hence, the second term on the r.h.s. of Eq. 9 is caused by the class overlap and it can be used to approximate the Bayes risk. Put together, the first term of the decomposition reflects the missing knowledge on the optimal value of θ that can be reduced by increasing the training set size, while the second reflects the uncertainty stemming from the properties of the true data distribution. Hence we refer to the first term as the *reducible model uncertainty* and the second the *data uncertainty*.

Evidential Bayesian Models. In all the analysis above, we assumed a fixed and unknown π that modulates the whole process via and cannot be identified by the learning scheme. When we characterize the uncertainty on the class distribution by a prior belief $\pi \sim p(\pi)$, we attain the joint $p(y, \pi|x) = Pr[y|x, \pi]p(\pi|x)$. The variance of the Bayes optimal classifier that averages over this uncertainty $Pr[y|x] = \int Pr[y|x, \pi]p(\pi|x)d\pi$ decomposes as

$$Var[y=k|x] = \underbrace{Var_{\pi\sim p(\pi|x)}[f^{\pi,k}_{true}(x)]}_{\text{Irreducible model uncertainty}} + \underbrace{\mathbb{E}_{\pi\sim p(\pi|x)}\left[(1-f^{\pi,k}_{true}(x))f^{\pi,k}_{true}(x)\right]}_{\text{Data uncertainty}}.$$

The main source of uncertainty $p(\pi|x)$ is not a posterior this time but an empirical prior on a single observation x hence its variance will not shrink as $|\mathcal{D}_{tr}| \to +\infty$. Therefore the first term on the r.h.s. reflects the *irreducible model uncertainty* caused by the missing knowledge about π. The second term indicates data uncertainty as in PBMs, but accounts for the local uncertainty at x caused by π. *Evidential Bayesian Models (EBMs)* suggest the below approximation (Sensoy et al., 2018; Malinin & Gales, 2018)

$$p(y, \pi|x) = Pr[y|x, \pi]p(\pi|x) \approx Pr[y|\pi]q_\psi(\pi|x)$$

where $q_\psi(\pi|x)$ is a parametric model and the dependency of the class-conditional on the input is dropped. Note that the resultant model employs uncertainty on individual data points via π, but it does not have any global random variables. The standard evidential model training is performed by maximizing the expected likelihood subject to a regularizer that penalizes the divergence of $q_\psi(\pi|x)$ from the prior belief

$$\underset{\psi}{\operatorname{argmin}} - \int \log Pr[y|\pi]q_\psi(\pi|x)d\pi + \beta KL(q_\psi(\pi|x)||p(\pi)).$$

Although presented in the original work as as-hoc design choices, such a training objective can alternatively be viewed as $\beta-$regularized (Higgins et al., 2017) variational inference of $Pr[y|\pi]p(\pi|x)$ with the approximate posterior $q_\psi(\pi|x)$.

4 Complete Bayesian Models: Best of Both Worlds

The aforementioned uncertainty decomposition characteristics of PBMs and EBMs provide complementary strengths towards achieving total calibration, namely:

Model misfit $\Rightarrow$ PBM $>$ EBM. PBM is favorable because: i) shrinking posterior variance with growing training set size (Eq. 8 and the recovery of θ_{MLE} which inherits the consistency guarantees the frequentist approach. Since the uncertainty on the local variable π does not shrink for large samples, NLL would measure how well ψ can capture the regularities of heteroscedastic noise across individual samples, which is a more difficult task than quantifying the fit of a parametric model.

Class overlap $\Rightarrow$ EBM $>$ PBM. EBM is favorable because: i) the data uncertainty term of EBM $\mathbb{E}_{\pi\sim p(\pi|x_*)}[(1-h^{\theta}_{\pi,k}(x_*))h^{\theta}_{\pi,k}(x_*)]$ is likely to have less estimator variance than $\mathbb{E}_{\theta\sim p(\theta|\mathcal{D}_{tr})}[(1-h^{\theta}_{\pi,k}(x_*))h^{\theta}_{\pi,k}(x_*)]$ and ii) the calculation of $p(\pi|x_*)$ does not require approximate posterior inference as for $p(\theta|\mathcal{D}_{tr})$.

Domain mismatch $\Rightarrow$ PBM $>$ EBM. PBM is favorable because the effect of the modulation of a global θ on the variance of Z applies also to the posterior predictive distribution with the only difference that x_* is a test sample. When the test sample is away from the training set, i.e. $\min_{x \in \mathcal{D}_{tr}} ||x_* - x||$ is large, then $p(y_*|x_*, \theta)$ is less likely to superpose with those regions of θ where $L(\theta)$ is pronounced, hence will be flattened out leading to a higher variance posterior predictive for samples coming from another domain. Since EBM has only local random variables, the variance of its posterior is less likely to build a similar discriminative property for domain detection.

As a result of the observations above, we arrive at the below hypothesis.

Main Hypothesis. *A model that inherits the model uncertainty of PBM and data uncertainty of EBM will be most capable of solving tasks 1,2,3.*

Guided by our main hypothesis, we combine the PBM and EBM designs within a unified framework that inherits the desirable uncertainty quantification properties of each individual approach

$$Pr[y|\pi]p(\pi|\theta, x)p(\theta), \tag{10}$$

which we refer to as a *Complete Bayesian Model (CBM)* hinting to its capability to solve the total calibration problem. The model simply introduces a global random variable θ into the empirical prior $p(\pi|\theta, x)$ of the EBM. The variance of the posterior predictive of the resultant model decomposes as

$$\begin{aligned} Var[y = k|x] = & \underbrace{Var_{p(\theta|\mathcal{D})}\Big[\mathbb{E}_{p(\pi|x,\theta)}[\mathbb{E}[y|\pi, x]]\Big]}_{\text{Reducible Model Uncertainty}} + \underbrace{\mathbb{E}_{p(\theta|\mathcal{D})}\Big[Var_{p(\pi|\theta,x)}[\mathbb{E}[y|\pi]]\Big]}_{\text{Irreducible Model Uncertainty}} \\ & + \underbrace{\mathbb{E}_{p(\theta|\mathcal{D})}\Big[\mathbb{E}_{p(\pi|x,\theta)}[Var[y = k|\pi]]\Big]}_{\text{Data Uncertainty}} \end{aligned} \tag{11}$$

where the r.h.s. of the decomposition has the following desirable properties: i) The first term recovers the form of the reducible model uncertainty term of PBM when π is marginalized $Var_{p(\theta|\mathcal{D})}[\mathbb{E}_{p(\pi|x,\theta)}[\mathbb{E}[y|\pi, x]]] = Var_{p(\theta|\mathcal{D})}[\mathbb{E}[y|\theta, x]]$. ii) The second term is the irreducible model uncertainty term of EBM averaged over the uncertainty on the newly introduced global variable θ. It quantifies the portion of uncertainty stemming from heteroscedastic noise, which is not explicit in the decomposition of PBM. iii) The third term recovers the data uncertainty term of EBM when θ is marginalized: $\mathbb{E}_{p(\theta|\mathcal{D})}[\mathbb{E}_{p(\pi|x,\theta)}[Var[y|\pi]] = \mathbb{E}_{p(\pi|x)}[Var[y|\pi]]$.

5 The Evidential Turing Process: An Effective CBM Realization

Equipping the empirical prior $p(\pi|\theta, x)$ of CBM with the capability of *learning* to generate accurate prior beliefs on individual samples is the key for total calibration. We adopt the following two guiding principles to obtain highly expressive empirical priors:

- The existence of a global random variable θ can be exploited to express complex reducible model uncertainties using the Neural Processes (Garnelo et al., 2018b) framework.
- The conditioning of $p(\pi|\theta, x)$ on a global variable θ and an individual observation x can be exploited with an attention mechanism where θ is a memory and x is a query. Dependency on a context set during test time can be lifted using the Neural Turing Machine (Graves et al., 2014) design, which maintains an external memory that is updated by a rule detached from the optimization scheme of the main loss function.

We extend the stochastic process derivation of the Neural Processes by marginalizing out a local variable from a PBM with an external memory that follows the Neural Turing Machine design and arrive at a new family of stochastic processes called a *Turing Process,* formally defined as below.

Definition 1. *A Turing Process is a collection of random variables $Y = \{y_i | i \in \mathcal{I}\}$ for an index set $\mathcal{I} = \{1, \ldots, K\}$ with arbitrary $K \in \mathbb{N}^+$ that satisfy the two properties*

$$\textit{(i)}\ p_M(Y) = \int \prod_{y_i \in Y} p_M(y_i|\theta)p_M(\theta)d\theta, \quad \textit{(ii)}\ p_{M'}(Y|Y') = \int \prod_{y_i \in Y} p(y_i|\theta)p_{M'}(\theta|Y')d\theta,$$

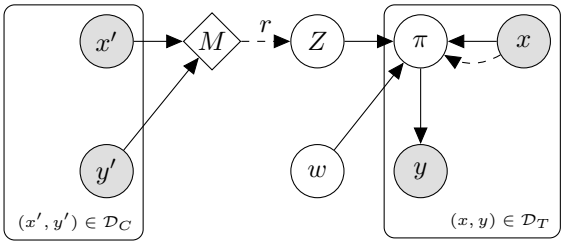

(a) ETP Plate diagram

while *Model not converged* **do**
  for $\mathcal{D}_{batch} \subset \mathcal{D}$ **do**
    Choose $\mathcal{D}_C \subset \mathcal{D}_{batch}$
    $M \leftarrow$
    $\mathbb{E}_{Z \sim p_M(Z)} [r(Z, \mathcal{D}_C)]$
    $\lambda \leftarrow \lambda - \nabla_\lambda \mathcal{F}_{ETP}(\lambda)$
  end
end

(b) ETP Training

Figure 2: The Evidential Turing Process: *(left)* The essential design choice is how $p(\pi|Z, w, x)$ is constructed thanks to an external memory M that can be queried with respect to any input x without needing to store context data at test time. The dashed arrow indicates that Z can condition on a context $\mathcal{D}_C$ by updates its parameters M with an explicit function r. *(right)* The ETP training routine.

for another random variable collection Y' of arbitrary size that lives in the same probability space as Y, a probability measure $p_M(\theta)$ with free parameters M and some function $M' = r(M, Y')$.

The Turing Process can express all stochastic processes since Property (i) is sufficient to satisfy the Kolmogorov's Extension Theorem (Øksendal, 1992) and choosing r simply to be an identity mapping would revert us back to the generic definition of a stochastic process. The Turing Process goes further by permitting to explicitly specify how information accumulates within the prior. This is a different approach from the Neural Process that performs conditioning $p(Y|Y')$ by applying an amortized posterior $q(\theta|Y')$ on a plain stochastic process that satisfies only Property (i), hence maintains a data-agnostic prior $p(\theta)$ and depends on a context set also at the prediction time.

Given a disjoint partitioning of the data $\mathcal{D} = \mathcal{D}_C \cup \mathcal{D}_T$ into a context set $(x', y') \in \mathcal{D}_C$ and a target set $(x, y) \in \mathcal{D}_T$, we propose the data generating process on the target set below

$$p(y, \mathcal{D}_T, \pi, \theta) = p(w) \underbrace{p_M(Z)}_{\substack{\text{External} \\ \text{memory}}} \prod_{(x,y) \in \mathcal{D}_T} \{p(y|\pi) \underbrace{p(\pi|Z, w, x)}_{\substack{\text{Input-specific} \\ \text{prior}}}\}. \tag{12}$$

We decouple the global parameters $\theta = \{w, Z\}$ into w that parameterizes a mapping from the input to the hyperparameter space and an external memory $Z = \{z_1, \ldots, z_R\}$ governed by the distribution $p_M(Z)$ parameterized by M that stores a fixed-sized summary of the context data observed during training. The memory variable Z can update its belief conditioned on the context set $\mathcal{D}_C$ by updating its parameters with an explicit rule $p_M(Z|\mathcal{D}_C) \leftarrow p_{\mathbb{E}_{Z \sim p_M(Z)}[r(Z, \mathcal{D}_C)]}(Z)$. The hyperpriors of $p(\pi|Z, w, x)$ are then determined by querying the memory Z for each input observation x using an attention mechanism, for instance a transformer network (Vaswani et al., 2017). Choosing the variational distribution as $q_\lambda(\theta, \pi|x) = q_\lambda(w) p_M(Z) q(\pi|Z, w, x)$, we attain the variational free energy formula for our target model

$$\mathcal{F}_{ETP}(\lambda) = \tag{13}$$
$$\mathbb{E}_{q_\lambda(w)} \left[-\sum_{(x,y) \in \mathcal{D}} \mathbb{E}_{q_\lambda(\pi|Z,w,x)} \left[\mathbb{E}_{p_M(Z)} \left[\log p(y|\pi) + \log \frac{q_\lambda(\pi|Z, w, x)}{p(\pi|Z, w, x)} \right] \right] + \log \frac{q_\lambda(w)}{p(w)} \right].$$

The learning procedure will then alternate between updating the variational parameters λ via gradient-descent on $\mathcal{F}_{ETP}(\lambda)$ and updating the parameters of the memory variable Z via an external update rule as summarized in Figure 2b. ETP can predict a test sample (x_*, y_*) by only querying the input x_* on the memory Z and evaluating the prior $p(\pi_*|Z, w, x_*)$ without need for any context set as

$$p(y_*|\mathcal{D}_{tr}, x_*) \approx \iint p(y_*|\pi_*) q(\pi_*|Z, w, x_*) p_M(Z) q_\lambda(w) dZ dw. \tag{14}$$

Table 1: **Ablation Table.** Deactivating the components of ETP one at a time equates it to state-of-the-art methods. We curate ENP as a surrogate for the Attentive NP (ANP) of (Kim et al., 2019), which requires test-time context, and an improved NP variant with reduced estimator variance thanks to π.

Model	π	Z	M	r	$\mathcal{D}_c^{(test)}$	Compare
ETP (Target)	✓	✓	✓	✓	×	
ANP (Kim et al., 2019)	✓	✓	✓	×	✓	No
ENP (Surrogate)	✓	✓	×	×	×	Yes
NP (Garnelo et al., 2018b)	×	✓	×	×	×	No
EDL (Sensoy et al., 2018)	✓	×	×	×	×	Yes
BNN (Molchanov et al., 2017)	×	×	×	×	×	Yes

✓: Component active ×: Component inactive

$\mathcal{D}_c^{(test)}$: Demand for context data at test time

6 Most Important Special Cases of the Evidential Turing Process

As we build the design of ETP on the CBM framework that over-arches the prevalent parametric and evidential approaches, its ablation amounts to recovering many state-of-the-art modeling approaches as listed in Table 1 and detailed below.

Bayesian Neural Net (BNN) (Neal, 1995; MacKay, 1992; 1995) is the most characteristic PBM example that parameterizes a likelihood $p(y|\theta, x)$ with a neural network $f_\theta(\cdot)$ whose weights follow a distribution $\theta \sim p(\theta)$. We adopt the following data generating process for classification $\theta \sim \mathcal{N}(\theta|0, \beta^{-1}I)$ and infer its posterior by mean-field variational posterior $q_\lambda(\theta)$ applying the reparameterization trick (Kingma et al., 2015; Molchanov et al., 2017).

Evidential Deep Learning (EDL) (Sensoy et al., 2018), the characteristic example of EBMs, employs an uninformative Dirichlet prior on the class probabilities, which then set the mean of a normal distribution on the one-hot-coded class labels $y, \pi \sim \mathcal{D}ir(\pi|1, \dots, 1)\mathcal{N}(y|\pi, 0.5I_K)$. EDL links the input observations to the distribution of class probabilities by performing amortized variational inference with the approximate distribution $q_\lambda(\pi; x) = \mathcal{D}ir(\pi|\alpha_\lambda(x))$.

Neural Processes (NP) (Garnelo et al., 2018a;b) are PBMs used to generate stochastic processes from neural networks by integrating out the global parameters θ as in Property (i) of Definition 1. NPs differ from PBMs by amortizing an arbitrary sized context set $\mathcal{D}_C$ on the global parameters $q(\theta|\mathcal{D}_C)$ via an aggregator network during inference. NPs can be viewed as Turing Processes with an identity map r. Follow-up work equipped NPs with attention (Kim et al., 2019), translation equivariance (Gordon et al., 2020; Foong et al., 2020), and sequential prediction (Singh et al., 2019; Yoon et al., 2020). All of these NP variants assume prediction-time access to context, making them suitable for interpolation tasks such as image in-painting but not for generic prediction problems.

Evidential Neural Processes (ENPs) is the EBM variant of a neural process we curate to bring together best practices of EDL and NPs and make the strongest possible baseline for ETP, defined as

$$p(y, \pi, Z|\mathcal{D}_C) = \mathcal{C}at(y|\pi)\mathcal{D}ir\big(\pi|\alpha_\theta(Z)\big)\mathcal{N}\big(Z|(\mu, \sigma^2) = r(\{h_\theta(x_j, y_j) \mid (x_j, y_j) \in \mathcal{D}_C\})\big), \quad (15)$$

with an aggregation rule $r(\cdot)$, an encoder net $h_\theta(\cdot, \cdot)$, and a neural net $\alpha_\theta(\cdot)$ mapping the global variable Z to the probability simplex. We further improve ENP with an attentive NP approach (Kim et al., 2019) by replacing the fixed aggregation rule r with an attention mechanism, thereby allowing the model to switch focus depending on the target. At the prediction time, we use $Z \sim \mathcal{N}(Z|\mathbf{1}, \kappa^2 I)$ for some small κ to induce an uninformative prior on π in the absence of a context set.

7 CASE STUDY: CLASSIFICATION WITH EVIDENTIAL TURING PROCESSES

We demonstrate a realization of an Evidential Turing Process to a classification problem below

$$y, \pi, w, Z|M \sim Cat(y|\pi)\mathcal{D}ir\big(\pi|\exp(a(v_w(x); Z))\big)\mathcal{N}(v|0, \beta^{-1}I)\prod_{r=1}^{R}\mathcal{N}(z_r|m_r, \kappa^2 I). \quad (16)$$

The global variable Z is parameterized by the memory $M = (m_1, \ldots, m_R)$ consisting of R cells $m_r \in \mathbb{R}^K$.[1] The input data x is mapped to the same space via an encoding neural net $v_w(\cdot)$ parameterizing a Dirichlet distribution over the class probabilities π via an attention mechanism $a(v_w, z) = \sum_{z' \in Z} \phi(v_w(x), z')z$, where $\phi(v_w(x), z) = \text{softmax}(\{k_\psi(z)^\top v_w(x)/\sqrt{K}|z \in Z\})$. The function $k_\psi(\cdot)$ is the key generator network operating on the embedding space. We update the memory cells as a weighted average between remembering and updating

$$m \leftarrow \mathbb{E}_{Z\sim p(Z|M)}\left[\tanh(\gamma m + (1-\gamma)\sum_{(x,y)\in\mathcal{D}_C}\phi(v_w(x), z)(\text{onehot}(y) + \text{soft}(v_w(x))))\right] \quad (17)$$

where $\gamma \in (0, 1)$ is a fixed scaling factor controlling the relative importance. The second term adds new information to the cell as a weighted sum over all pairs (x, y), taking both the true label (via $\text{onehot}(y)$) as well as the uncertainty in the prediction (via $\text{soft}(v_\theta(x))$) into account. The final $\tanh(\cdot)$ transformation ensures that the memory content remains in a fixed range across updates, as practised in LSTMs (Hochreiter & Schmidhuber, 1997).

8 EXPERIMENTS

We benchmark ETP against the state of the art addressed in the the ablation plan in Table 1 according to the total calibration criteria developed in Sec. 2 on four real-world data sets. See the Appendix B for full details on the experimental setup in each case and for the hyperparameters used throughout. We provide a reference implementation of the proposed model and the experimental pipeline.[2]

Total calibration. Table 2 reports the prediction error and the three performance scores introduced in Sec. 2 that constitute total calibration. We perform the out-of-domain detection task as in Malinin & Gales (2018) and classify the test split of the target domain and a data set from another domain based on the predictive entropy. ETP is the only method that consistently ranks among top performers in all data sets with respect to all performance scores, which supports our main hypothesis that CBM should outperform PBM and EBM in total calibration.

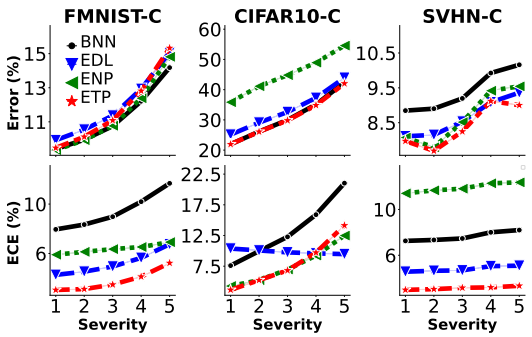

Figure 3: Results averaged across 19 types of corruption (e.g. motion blur, fog, pixelation) applied on the test splits of FMNIST, CIFAR10, and SVHN at five severity levels.

Response to gradual domain shift. In order to assess how well models can cope with a gradual transition from their native domain, we evaluate their ECE performance on data perturbed by 19 types of corruption Hendrycks & Dietterich (2019) at five different severity levels. Figure 3 depicts the performance of models averaged across all corruptions. ETP gives the best performance nearly in all data sets and distortion severity levels (see Appendix B.3 Table 4 for a tabular version of these results).

Computational cost. We measured the average wall-clock time per epoch in CIFAR10 to be 10.8 ± 0.1 seconds for ETP, 8.2 ± 0.1 seconds for BNN, 8.6 ± 0.1 seconds for EDL, and 9.5 ± 0.2 seconds for ENP. The relative standings of the models remain unchanged in all the other data sets.

[1] In the experiments we fix $\kappa^2 = 0.1$. Preliminary results showed stability as well for larger/smaller values.

[2] *Hidden to keep anonymity*

Table 2: Quantitative results on four data sets showing mean $\pm$ standard deviation across 10 repetitions. Best performing models that overlap within three standard deviations are highlighted in bold.

Domain Data (Architecture)	**IMDB** (LSTM)	**Fashion** (LeNet5)	**SVHN** (LeNet5)	**CIFAR10** (LeNet5)	**CIFAR100** (ResNet18)
Prediction accuracy as % test error					
BNN	**16.4** $\pm$**0.6**	**7.9**$\pm$**0.1**	7.9$\pm$0.1	**15.3**$\pm$**0.3**	30.2 $\pm$0.3
EDL	38.3 $\pm$13.3	8.6$\pm$0.1	7.3$\pm$0.1	18.5$\pm$0.2	45.2 $\pm$0.4
ENP	50.0 $\pm$0.0	**7.9**$\pm$**0.2**	**6.7**$\pm$**0.1**	**14.8**$\pm$**0.2**	39.0 $\pm$0.3
ETP (Target)	**15.8** $\pm$**1.3**	**7.9**$\pm$**0.2**	**6.9**$\pm$**0.1**	**15.3**$\pm$**0.2**	**29.2** $\pm$**0.3**
In-domain calibration as % Expected Calibration Error (ECE)					
BNN	14.4 $\pm$0.4	6.7$\pm$0.	6.5$\pm$0.	5.5$\pm$0.3	15.2$\pm$0.0
EDL	41.1 $\pm$2.6	3.7$\pm$0.2	4.0$\pm$0.1	9.0$\pm$0.2	**5.3**$\pm$**0.4**
ENP	**0.8** $\pm$**1.6**	6.0$\pm$0.2	10.7$\pm$0.2	7.2$\pm$0.3	39.7$\pm$0.4
ETP (Target)	**3.1** $\pm$**0.4**	**2.6**$\pm$**0.2**	**2.6**$\pm$**0.1**	**2.7**$\pm$**0.1**	6.6$\pm$0.1
Model fit as negative test log-likelihood					
BNN	0.47 $\pm$0.0	0.65$\pm$0.0	0.71$\pm$0.0	0.50$\pm$0.0	1.78$\pm$0.0
EDL	0.66 $\pm$0.1	0.37$\pm$0.0	0.34$\pm$0.0	0.72$\pm$0.0	2.24$\pm$0.0
ENP	0.69 $\pm$0.0	0.34$\pm$0.0	0.33$\pm$0.0	0.50$\pm$0.0	2.52$\pm$0.0
ETP (Target)	**0.37** $\pm$**0.0**	**0.29**$\pm$**0.0**	**0.26**$\pm$0.0	**0.46**$\pm$**0.0**	**1.36**$\pm$**0.0**
Out-of-domain detection as % Area Under ROC Curve					
OOD Data	Random	MNIST	CIFAR100	SVHN	TinyImageNet
BNN	**60.9** $\pm$**4.2**	75.9$\pm$2.3	86.2$\pm$0.5	**84.1**$\pm$**1.3**	97.2$\pm$0.5
EDL	**55.1** $\pm$**5.1**	77.5$\pm$2.0	90.9$\pm$0.3	79.2$\pm$0.7	89.6$\pm$0.3
ENP	**53.7** $\pm$**5.7**	**88.9**$\pm$**1.0**	**92.4**$\pm$**0.4**	**81.4**$\pm$**0.8**	**100.0**$\pm$**0.1**
ETP (Target)	**59.1** $\pm$**5.1**	**90.0**$\pm$**0.9**	90.0$\pm$0.4	**82.1**$\pm$**0.6**	99.6$\pm$0.1

9 Conclusion

Summary. We initially developed the first formal definition of total calibration. Then we analyzed how the uncertainty characteristics of two mainstream Bayesian modeling approaches are affected from their design. Next we introduced Complete Bayesian Models as a unifying framework that inherits the complementary strengths existing ones. We developed the Evidential Turing Process as an optimal realization of Complete Bayesian Models. We derived an experiment setup from our formal definition of total calibration and a systematic ablation of our target model into the strongest representatives of the state of the art. We observed in four real-world tasks that the Evidential Turing Process is the only model that can excel all three aspects of total calibration simulatenously.

Broad impact. Our work delivers evidence for the claim that epistemic awareness of a Bayesian model is indeed a capability learnable only from in-domain data, as appears in biological intelligence via closed-loop interactions of neuronal systems with stimuli. The implications of our work could follow up in interdisciplinary venues, with focus on the relation of associative memory and attention to the neuroscientific roots of epistemic awareness (Lorenz, 1978).

Limitations and ethical concerns. While we observed ETP outperform BNN variants in our experiments, whether BNNs could bridge the gap after further improvements in the approximate inference remains to be researched. The attention mechanism of ETP could also be improved, for instance to transformer nets (Vaswani et al., 2017). The explainability of the memory content of ETP deserves further investigation. The generalizeability of our results to very deep architectures, such as ResNet 152 or DenseNet 161 could be a topic of a separate large-scale empirical study. ETP does not improve the explainability and fairness of the decisions made by the underlying design choices, such as the architecture of the used neural nets in the pipeline. Potential negative societal impacts of deep neural net classifiers stemming from these two factors need to be circumvented separately before the real-world deployment of our work.

REFERENCES

Milton Abramowitz and Irene A. Stegun. *Handbook of Mathematical Functions*. Dover, 1965.

Andrew Foong, Wessel Bruinsma, Jonathan Gordon, Yann Dubois, James Requeima, and Richard Turner. Meta-Learning Stationary Stochastic Process Prediction with Convolutional Neural Processes. In *Advances in Neural Information Processing Systems*, 2020.

Marta Garnelo, Dan Rosenbaum, Christopher Maddison, Tiago Ramalho, David Saxton, Murray Shanahan, Yee Whye Teh, Danilo Rezende, and S. M. Ali Eslami. Conditional Neural Processes. In *International Conference on Machine Learning*, 2018a.

Marta Garnelo, Jonathan Schwarz, Dan Rosenbaum, Fabio Viola, Danilo J Rezende, SM Eslami, and Yee Whye Teh. Neural Processes. *Theoretical Foundations and Applications of Deep Generative Models workshop*, 2018b.

Jonathan Gordon, Wessel P. Bruinsma, Andrew Y. K. Foong, James Requeima, Yann Dubois, and Richard E. Turner. Convolutional Conditional Neural Processes. In *International Conference on Learning Representations*, 2020.

Alex Graves, Greg Wayne, and Ivo Danihelka. Neural Turing Machines. *arXiv preprint arXiv:1410.5401*, 2014.

Chuan Guo, Geoff Pleiss, Yu Sun, and Kilian Q. Weinberger. On Calibration of Modern Neural Networks. In *International Conference on Machine Learning*, 2017.

Dan Hendrycks and Thomas Dietterich. Benchmarking neural network robustness to common corruptions and perturbations. *Proceedings of the International Conference on Learning Representations*, 2019.

Irina Higgins, Loic Matthey, Arka Pal, Christopher Burgess, Xavier Glorot, Matthew Botvinick, Shakir Mohamed, and Alexander Lerchner. beta-VAE: Learning Basic Visual Concepts with a Constrained Variational Framework. In *Internationl Conference on Learning Representations*, 2017.

Sepp Hochreiter and Jürgen Schmidhuber. Long Short-Term Memory. *Neural Computation*, 9(8): 1735–1780, 1997.

Hyunjik Kim, Andriy Mnih, Jonathan Schwarz, Marta Garnelo, Ali Eslami, Dan Rosenbaum, Oriol Vinyals, and Yee Whye Teh. Attentive Neural Processes. In *International Conference on Learning Representations*, 2019.

Diederik P Kingma and Jimmy Ba. Adam: A method for stochastic optimization. *arXiv preprint arXiv:1412.6980*, 2014.

Diederik P. Kingma, Tim Salimans, and Max Welling. Variational Dropout and the Local Reparameterization Trick. *Advances in Neural Information Processing Systems*, 2015.

Alex Krizhevsky, Geoffrey Hinton, et al. Learning multiple layers of features from tiny images. 2009.

Volodymyr Kuleshov, Nathan Fenner, and Stefano Ermon. Accurate Uncertainties for Deep Learning using Calibrated Regression. In *International Conference on Machine Learning*, 2018.

Yann LeCun, Corinna Cortes, and CJ Burges. MNIST handwritten digit database. *ATT Labs [Online]. Available: http://yann.lecun.com/exdb/mnist*, 2, 2010.

Konrad Lorenz. *Die Rückseite des Spiegels: Versuch einer Naturgeschichte menschlichen Erkennens*. Piper, 1978.

Andrew L. Maas, Raymond E. Daly, Peter T. Pham, Dan Huang, Andrew Y. Ng, and Christopher Potts. Learning word vectors for sentiment analysis. In *Proceedings of the 49th Annual Meeting of the Association for Computational Linguistics: Human Language Technologies*, pp. 142–150, Portland, Oregon, USA, June 2011. Association for Computational Linguistics. URL http://www.aclweb.org/anthology/P11-1015.

David JC MacKay. A practical Bayesian framework for backpropagation networks. *Neural Computation*, 1992.

David JC MacKay. Probable Networks and Plausible Predictions – A Review of Practical Bayesian Methods for Supervised Neural Networks. *Network: Computation in Neural Systems*, 1995.

Andrey Malinin and Mark Gales. Predictive Uncertainty Estimation via Prior Networks. In *Advances in Neural Information Processing Systems*, 2018.

Dmitry Molchanov, Arsenii Ashukha, and Dmitry Vetrov. Variational Dropout Sparsifies Deep Neural Networks. In *International Conference on Machine Learning*, 2017.

Mahdi Pakdaman Naeini, Gregory Cooper, and Milos Hauskrecht. Obtaining well Calibrated Probabilities using Bayesian Binning. In *AAAI Conference on Artificial Intelligence*, 2015.

Radford Neal. *Bayesian Learning for Neural Networks*. PhD thesis, 1995.

Yuval Netzer, Tao Wang, Adam Coates, Alessandro Bissacco, Bo Wu, and Andrew Y. Ng. Reading Digits in Natural Images with Unsupervised Feature Learning. 2011.

Bernt Øksendal. *Stochastic Differential Equations: An Introduction with Applications*. Springer-Verlag, 1992.

Adam Paszke, Sam Gross, Francisco Massa, Adam Lerer, James Bradbury, Gregory Chanan, Trevor Killeen, Zeming Lin, Natalia Gimelshein, Luca Antiga, Alban Desmaison, Andreas Kopf, Edward Yang, Zachary DeVito, Martin Raison, Alykhan Tejani, Sasank Chilamkurthy, Benoit Steiner, Lu Fang, Junjie Bai, and Soumith Chintala. PyTorch: An Imperative Style, High-Performance Deep Learning Library. In *Advances in Neural Information Processing Systems 32*. 2019.

Herbert Robbins and Sutton Monro. A Stochastic Approximation Method. *The Annals of Mathematical Statistics*, 22(3):400 – 407, 1951. doi: 10.1214/aoms/1177729586. URL https://doi.org/10.1214/aoms/1177729586.

Gesina Schwalbe and Martin Schels. A Survey on Methods for the Safety Assurance of Machine Learning Based Systems. In *European Congress on Embedded Real Time Software and Systems*, 2020.

Murat Sensoy, Lance Kaplan, and Melih Kandemir. Evidential Deep Learning to Quantify Classification Uncertainty. In *Advances in Neural Information Processing Systems*, 2018.

Gautam Singh, Jaesik Yoon, Youngsung Son, and Sungjin Ahn. Sequential Neural Processes. In *Advances in Neural Information Processing Systems*, 2019.

Ashish Vaswani, Noam Shazeer, Niki Parmar, Jakob Uszkoreit, Llion Jones, Aidan N Gomez, Ł ukasz Kaiser, and Illia Polosukhin. Attention is All you Need. In *Advances in Neural Information Processing Systems*, 2017.

Han Xiao, Kashif Rasul, and Roland Vollgraf. Fashion-MNIST: a Novel Image Dataset for Benchmarking Machine Learning Algorithms. 2017.

Jaesik Yoon, Gautam Singh, and Sungjin Ahn. Robustifying Sequential Neural Processes. In *International Conference on Machine Learning*, 2020.

APPENDIX

A FURTHER THEORETICAL RESULTS AND DERIVATIONS

A.1 KULLBACK LEIBLER BETWEEN TWO DIRICHLET DISTRIBUTIONS

As our objective and the EDL baseline rely on the Kullback-Leibler divergence between two Dirichlet distributions, we repeat here for completeness the general form. Assuming two distributions over a K-dimensional probability π, $\mathcal{D}ir(\pi|\alpha)$ and $\mathcal{D}ir(\pi|\beta)$, parameterized by $\alpha, \beta \in \mathbb{R}_+^K$, we have

$$\text{KL}\left(\mathcal{D}ir(\pi|\alpha) \parallel \mathcal{D}ir(\pi|\beta)\right) = \log\left(\frac{\Gamma(\sum_k \alpha_k)\prod_k \Gamma(\beta_k)}{\Gamma(\sum_k \beta_k)\prod_k \Gamma(\alpha_k)}\right) + \sum_k (\alpha_k - \beta_k)\big(\psi(\alpha_k) - \psi(\textstyle\sum_k \alpha_k)\big),$$

where $\Gamma(\cdot)$ and $\psi(a) := \frac{d}{da}\log\Gamma(a)$ are the *gamma* and *digamma* functions (Abramowitz & Stegun, 1965).

A.2 THE EVIDENTIAL DEEP LEARNING OBJECTIVE

The analytical solutions for the Evidential Deep Learning (Sensoy et al., 2018) loss as defined in the main paper can be computed as follows. For a single K-dimensional observation y, dropping the n from the notation and instead using the index for the dimensionality throughout the following equations, we have that the expectation in the expectation terms are given as

$$\begin{aligned}
\mathbb{E}_{p(\pi|x)}\left[||y-\pi||^2\right] &= \mathbb{E}_{p(\pi|x)}\left[(y-\pi)^\top(y-\pi)\right] \\
&= \sum_{k=1}^{K} \mathbb{E}_{p(\pi|x)}\left[(y_k-\pi_k)^2\right] \\
&= \sum_{k=1}^{K} \mathbb{E}_{p(\pi|x)}\left[(y_k - \mathbb{E}_{p(\pi|x)}\left[\pi_k\right] + \mathbb{E}_{p(\pi|x)}\left[\pi_k\right] - \pi_k)^2\right] \\
&= \sum_{k=1}^{K} (y_k - \mathbb{E}_{p(\pi|x)}\left[\pi_k\right])^2 + \text{var}_{p(\pi|x)}\left[\pi_k\right],
\end{aligned}$$

with the tractable expectation and variance of a Dirichlet distributed π. The Kullback-Leibler term is between two Dirichlet distributions and given (see the general form in A.1) as

$$\begin{aligned}
&\text{KL}\left(\mathcal{D}ir(\pi|\alpha_\theta(x)) \parallel \mathcal{D}ir(\pi|1,\dots,1)\right) \\
&= \log\left(\frac{\Gamma\big(\sum_k \alpha_\theta(x)_k\big)}{\Gamma(K)\prod_k \Gamma(\alpha_\theta(x)_k)}\right) + \sum_{k=1}^{K}(\alpha_\theta(x)_k - 1)\Big(\psi(\alpha_\theta(x)_k) - \psi\big(\textstyle\sum_k \alpha_\theta(x)_k\big)\Big).
\end{aligned}$$

A.3 EVIDENTIAL DEEP LEARNING AS A LATENT VARIABLE MODEL

As discussed in the main paper for a set of N observations $\mathcal{D} = \{(x_1, y_1), \dots, (x_N, y_N)\}$, the objective EDL minimizes is given as

$$\mathcal{L}_{\text{EDL}} = \sum_{n=1}^{N} \mathbb{E}_{p(\pi_n|x_n)}\left[||y_n - \pi_n||_2^2\right] + \lambda \text{KL}\left(p(\pi_n|x_n) \parallel \mathcal{D}ir(\pi_n|1,\dots,1)\right),$$

where $p(\pi_n|x_n) = \mathcal{D}ir(\pi|\alpha_\theta(x_n))$. We can instead assume the following generative model

$$\begin{aligned}
\pi_n &\sim \mathcal{D}ir(\pi_n|1,\dots,1) \qquad \forall n \\
y_n &\sim \mathcal{N}(y_n|\pi_n, 0.5 I_K) \qquad \forall n,
\end{aligned}$$

i.e. latent variables π_n and K-dimensional observations y_n following a multivariate normal prior. Approximating the intractable posterior $p(\boldsymbol{\pi}|\mathbf{y})$, where $\boldsymbol{\pi} = (\pi_1, \dots, \pi_n)$, $\mathbf{y} = (y_1, ..., y_n)$, with an

amortized variational posterior $q(\pi_n; x_n) = \mathcal{D}ir(\pi_n|\alpha_\theta(x_n))$, where $\alpha_\theta(\cdot)$ is the same architecture as in the EDL model, we have as the *evidence lower bound (ELBO)* to be maximized

$$
\begin{aligned}
&\sum_{n=1}^{N} \mathbb{E}_{q(\pi_n;x_n)} \left[\log p(y_n|\pi_n)\right] - \mathrm{KL}\left(q(\pi_n; x_n) \parallel p(\pi_n)\right) \\
= &\sum_{n=1}^{N} \mathbb{E}_{q(\pi_n;x_n)} \left[-\frac{1}{2}\log(2\pi) + \frac{K}{2}\log(2) - (y_n - \pi_n)^\top (y_n - \pi_n)\right] - \mathrm{KL}\left(q(\pi_n; x_n) \parallel p(\pi_n)\right) \\
= &\ \text{const} - \sum_{n=1}^{N} \mathbb{E}_{q(\pi_n;x_n)} \left[(y_n - \pi_n)^\top (y_n - \pi_n)\right] - \mathrm{KL}\left(q(\pi_n; x_n) \parallel p(\pi_n)\right) \\
= &\ \text{const} - \mathcal{L}_{\text{EDL}},
\end{aligned}
$$

that is the negative ELBO is equal to the EDL loss up to an additive constant.

A.4 Posterior Predictive

The posterior predictive for y^* given a new observation x^* can be computed as

$$
p(y^* = k|x^*, \mathcal{D}) \approx \mathbb{E}_{p(Z|M)}\left[\mathbb{E}_{q_\lambda(\pi|x^*,Z)}\left[p(y^* = k|\pi)\right]\right] = \mathbb{E}_{p(Z|M)}\left[h_\theta^k / \textstyle\sum_{k'} h_\theta^{k'}\right],
$$

where $h_\theta^k = h_\theta\left(v_\theta(x^*), a(v_\theta(x^*); Z)\right)_k$. That is, we can compute it analytically up to a sampling-based evaluation of the expectation over $p(Z|M)$.

B Experimental Details

B.1 Synthetic 1D two-class classification

We illustrate the qualitative behaviour of ETP on a simple synthetic 1d two-class classification task. The data consist of observations (20 per class) from two highly overlapping Gaussian distributions. The neural net, a simple one hidden layer architecture, can learn the task reasonably well. Figure 4 shows the raw data and underlying distributions as well as the learned memory evidence. The model learns to place more evidence on the correct class further away from the decision boundary while also becoming more varied with increasing distance. Within the high-density region, the asymmetry in how the specific observations are spread out leads to an asymmetry in the memory evidence. Below zero, the blue points are well separated, leading to a quick emphasis on that class as we move towards the left. Above zero, however, some blue observations in the orange region prevent the model from rapidly developing overconfidence.

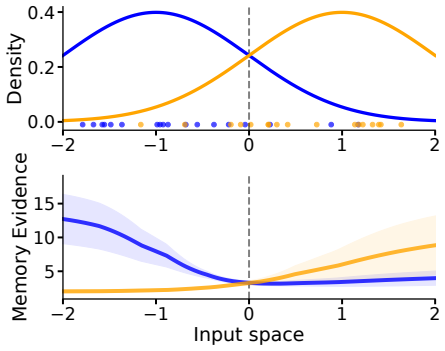

Figure 4: **1D Classification Task.** The upper plot shows the underlying distributions of each of the two classes, as well as the observed data. The lower shows the regularizing evidence the generative model places on each of the two classes depending on location in space, that is, mean $\pm$ one standard deviation over ten samples from $p(Z|M)$.

This synthetic data set consisting of two classes with 20 observations each sampled from standard normal distributions centered at ± 1 respectively. The encoding function $v_\phi(\cdot)$ consists of a multi-layer perceptron with a single hidden layer consisting of 32 neurons and a ReLU activation function. It is optimized for 400 epochs with the Adam optimizer (Kingma & Ba, 2014) using the PyTorch (Paszke et al., 2019) default parameters and a learning rate of $1e-3$. In order to keep the model as simple as possible, the key generator function $k_\lambda(\cdot)$

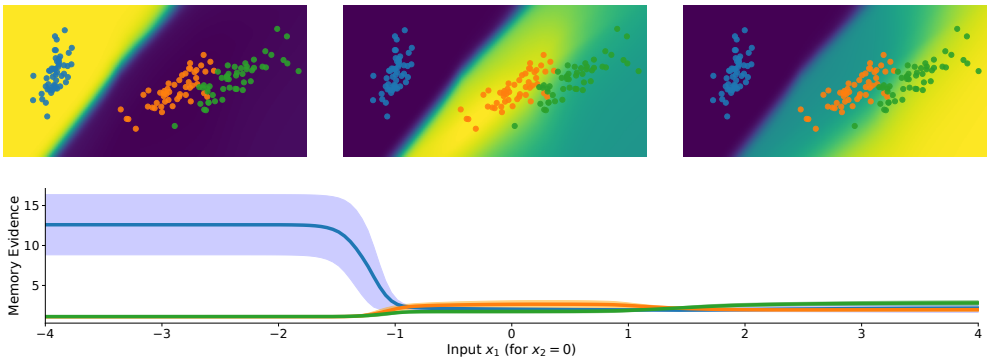

Figure 5: **2D Classification Task.** The three upper plots visualize the regularizing evidence that the model places on the location in space as the average over ten samples from $p(Z|M)$. The color scales are different across the three plots and vary in overall intensity. The lower plot visualizes a horizontal cut through the middle of these plots, putting them on a common scale. The solid lines in each color indicate the mean memory evidence, and the corresponding shaded areas indicate one standard deviation. Around the separable blue class, the memory strongly emphasizes the correct class with large confidence and suppresses the other two classes depicted in orange and green. While always preferring the correct class, the memory regularizes against overconfidence around the overlapping orange and green classes.

is constrained to being the identity function, while $h_\xi\big(v(x), a(v(x); Z)\big) = v(x) + \tanh(a(v(x); Z)$. The memory update is simplified to dropping the $\tanh(\cdot)$ rescaling.

B.2 Iris 2D three-class classification

The data set used in this experiment is the classical Iris data set[3] consisting of 150 samples of three iris species (50 per class), with four features measured per sample. We first map the data to the first two principal components for visualization and also use this modified version as the training data. This gives an interpretable toy learning setup where one class is clearly separated from the other two overlapping classes. The encoding function $v_\phi(\cdot)$ consists of an MLP with two hidden layers of 32 neurons each and ReLU activation functions. It is optimized for 400 epochs with the Adam optimizer using the PyTorch default parameters and a learning rate of $1e-3$. In order to keep the model as simple as possible, the key generator function $k_\lambda(\cdot)$ is constrained to being the identity function, while $h_\xi\big(v(x), a(v(x); Z)\big) = v(x) + \tanh(a(v(x); Z)$. The memory update is simplified to dropping the $\tanh(\cdot)$ rescaling.

Figure 5 shows the varying importance the model assigns to different parts of the input space depending on the class under consideration. For the separate blue class, the model is a lot more confident in relative terms and absolute values.

B.3 Image Classification Experiments

All experiments are implemented in PyTorch (Paszke et al., 2019) version 1.7.1 and trained on a TITAN RTX. They have been replicated ten times over random initial seeds. The experimental details are as follows:

Fashion MNIST (FMNIST) (Xiao et al., 2017). Uses a LeNet5-sized architecture (see Table 3). The out-of-distribution data is the MNIST (LeCun et al., 2010) data set. All data sets are z-score normalized given the in-domain mean and standard deviations. The training objective for each model

[3]Originally due to Fisher (1936) and Anderson (1935). We rely on the version provided by the `scikit learn` library, see `https://scikit-learn.org/stable/modules/classes.html#module-sklearn.datasets`.

Table 3: The neural network architectures used for the FMNIST, CIFAR10 and SVHN data set with ReLU activations between the layers.

FMNIST	CIFAR10/SVHN
Convolution (5×5) with 20 channels	Convolution (5×5) with 192 channels
MaxPooling (2×2) with stride 2	
Convolution (5×5) with 50 channels	Convolution (5×5) with 192 channels
MaxPooling (2×2) with stride 2	
Linear with 500 neurons	Linear with 1000 neurons
Linear with 10 neurons	

CIFAR100	
Layer Name	ResNet-18
Conv1	$7 \times 7, 64$, stride 2
	3×3 max pool, stride 2
Conv2_x	$\begin{bmatrix} 3 \times 3, 64 \\ 3 \times 3, 64 \end{bmatrix} \times 2$
Conv3_x	$\begin{bmatrix} 3 \times 3, 128 \\ 3 \times 3, 128 \end{bmatrix} \times 2$
Conv4_x	$\begin{bmatrix} 3 \times 3, 256 \\ 3 \times 3, 256 \end{bmatrix} \times 2$
Conv5_x	$\begin{bmatrix} 3 \times 3, 512 \\ 3 \times 3, 512 \end{bmatrix} \times 2$
Average Pool	7×7 average pool
Linear	100 neurons

IMDB	
Layer Name	LSTM
Embedding	$1001 \rightarrow 64$
LSTM	2 layers with 256 hidden size
Linear	2 neurons

is optimized via the Adam optimizer (Kingma & Ba, 2014) with a learning rate of $1e-3$. Each model is trained for 50 epochs.

CIFAR10 (C10) (Krizhevsky et al., 2009). Uses a LeNet5-sized architecture (see Table 3). The out-of-distribution data is the SVHN (Netzer et al., 2011). All data sets are z-score normalized given the in-domain mean and standard deviations. We further rely on data augmentation for the in domain data using random crops with 32 pixels and four pixel padding as well as horizontal flips. The training objective for each model is optimized via the Adam optimizer (Kingma & Ba, 2014) with a learning rate of $1e-4$. Each model is trained for 100 epochs.

SVHN (Netzer et al., 2011). Uses a LeNet5-sized architecture (see Table 3). The out-of-distribution data is the CIFAR10 (Krizhevsky et al., 2009) data set. All data sets are z-score normalized given the in-domain mean and standard deviations. The training objective for each model is optimized via the Adam optimizer (Kingma & Ba, 2014) with a learning rate of $1e-4$. Each model is trained for 100 epochs.

IMDB Sentiment Classification (Maas et al., 2011) Uses a LSTM architecture with 64 embedding dimensions and 2 layers with 256 hidden dimensions.. The out-of-distribution data is randomly generated. The training objective for each model is optimized via the SGD optimizer (Robbins & Monro, 1951) with a learning rate of 0.05 and 0.9 momentum. Each model is trained for 20 epochs. For data preparation part, we follow the notebook [4].

[4] available at https://www.kaggle.com/arunmohan003/sentiment-analysis-using-lstm-pytorch

Table 4: Quantitative results of models on the FMNIST-C, CIFAR10-C and SVHN-C test dataset using the LeNet5. The results shown mean ± three standard deviation.

		FMNIST-C		CIFAR10-C		SVHN-C	
Severity	Method	Err (%) (↓)	ECE (%) (↓)	(↓)	ECE (%) (↓)	(↓)	ECE (%) (↓)
1	BNN	**9.4**±2.8	8.0±2.4	**21.9**±4.5	**7.6**±2.9	**8.8**±1.2	7.3±1.0
	EDL	**9.9**±2.6	4.3±1.0	**25.1**±4.6	10.4±1.3	**8.1**±1.2	4.6±0.6
	ENP	**9.3**±2.7	5.9±0.5	35.9±6.0	**4.3**±1.7	**8.1**±1.3	11.4±1.0
	ETP	**9.5**±2.8	**3.0**±1.0	**21.9**±4.6	**3.6**±2.2	**8.0**±1.2	**3.0**±0.4
2	BNN	**9.9**±2.3	8.3±1.9	**26.1**±5.3	**10.0**±3.7	**8.9**±1.2	7.3±0.9
	EDL	**10.5**±2.1	**4.5**±0.8	**29.1**±5.1	**10.1**±1.6	**8.2**±1.1	4.6±0.6
	ENP	**9.9**±2.3	6.1±1.0	**41.1**±6.6	**5.2**±2.1	**7.8**±1.2	11.7±1.1
	ETP	**10.1**±2.4	**3.1**±0.8	**26.1**±5.3	**5.2**±2.8	**7.7**±1.1	**3.0**±0.5
3	BNN	**10.7**±2.3	9.0±1.9	**30.0**±7.6	**12.3**±5.3	**9.2**±1.6	7.5±1.2
	EDL	**11.4**±2.1	**4.9**±0.9	**32.6**±7.0	**9.8**±1.5	**8.5**±1.5	**4.7**±0.7
	ENP	**10.8**±2.3	6.4±1.6	**44.8**±9.0	**7.0**±3.4	**8.5**±1.7	11.8±1.5
	ETP	**11.1**±2.4	**3.5**±0.9	**29.8**±7.2	**6.8**±3.8	**8.2**±1.5	**3.2**±0.6
4	BNN	**12.2**±4.2	10.2±3.6	**35.1**±10.9	**15.9**±8.3	**9.9**±2.5	8.0±1.9
	EDL	**12.9**±4.2	**5.6**±1.8	**37.3**±10.0	**9.6**±1.4	**9.1**±2.4	**5.1**±1.0
	ENP	**12.4**±4.3	**6.5**±2.2	**48.9**±11.2	**9.2**±5.4	**9.4**±2.8	12.3±2.2
	ETP	**12.8**±4.6	**4.1**±1.8	**34.8**±10.3	**9.7**±6.4	**9.1**±2.4	**3.2**±1.0
5	BNN	**14.2**±5.4	**11.7**±4.6	**42.4**±13.7	21.0±10.4	**10.2**±2.5	8.2±1.9
	EDL	**15.1**±5.8	**6.7**±3.1	**43.9**±12.5	**9.5**±2.4	**9.4**±2.4	**5.1**±1.1
	ENP	**14.8**±6.5	**6.9**±3.1	**54.6**±12.7	**12.5**±7.0	**9.5**±2.8	12.4±2.3
	ETP	**15.3**±7.1	**5.2**±3.4	**42.1**±13.1	**14.1**±8.6	**9.0**±2.5	**3.3**±1.0

Shared Details and Observations. In all experiments, we train the BNN models with a cross-entropy loss, relying on the softmax for prediction. The EDL model is trained with the original loss (Sensoy et al., 2018). The prediction is made with the mean of the Dirichlet distribution like in the original work. In all models, entropy is used for detecting out-of-distribution instances.

Robustness against perturbations. The CIFAR10-C dataset is taken from the original work by Hendrycks & Dietterich (2019). As FMNIST-C and SVHN-C are not available, we created them are created following the same procedure as in the original work. For FMNIST the procedure, designed for three-channel RGB images, needs to be adapted to work with one-channel gray-scale images. To that end, we convert the gray-scale images to pseudo-RGB images by replicating the original gray channel three times. After applying the distortions, we transfer it again back into a one-channel gray-scale format. Table 4 gives the raw results used to create Figure 3 in the main paper.